Monte Carlo simulations of the decomposition of metastable solid solutions: Transient and steady-state nucleation kinetics

F. Soisson and G. Martin
Section de Recherches de Métallurgie Physique, DECM-SRMP, CEA Saclay, 91191 Gif-sur-Yvette Cedex, France
(Received 13 January 2000)

We present a study on the kinetics of coherent precipitation in weakly super-saturated substitutional solid solutions by the Monte Carlo method. Our simulations are based on a simple atomistic model of diffusion by vacancy jumps. The whole precipitation process (from early stages to late stage coarsening) is followed for various supersaturations and temperatures, and typical behaviors observed in the simulations are compared to those predicted by the classical theories. Special emphasis is placed on the first stages of the decomposition (incubation and nucleation) and on the effects of the vacancy diffusion mechanism. Finally we consider the addition of a third (impurity) element, which can be used to control the kinetic pathway: such effects are quantitatively explored with the Monte Carlo method.

I. INTRODUCTION

The decomposition of a metastable solid solution α by precipitation of a solute rich β phase is generally divided into three successive stages:[1] the nucleation of stable β clusters, their growth, and finally their coarsening. In this paper, we focus on the kinetics of the first steps, on the concepts of incubation time and nucleation rate, using simulations by the Monte Carlo method in the framework of a simple atomistic diffusion model.

The precipitation of a phase can be observed in many physical situations and it has been theoretically studied in a set of models known as the ''classical theory of nucleation'' (CTN), since the early works of Volmer and Weber (1926), Farkas (1927), Becker and Döring (1935), Frenkel (1939), and Zeldovitch (1942) (see Refs. 2–6 for extensive reviews, and references therein).

In these theories, the nucleation of the β clusters is controlled by a balance between a volumic decrease in free energy (Δf_v) and an increase due to an interfacial energy (σ). This leads to the concepts of critical size and nucleation barrier (see below). One of the main results is that, in a solid solution of initial supersaturation S_0, after a time lag (the so-called ''incubation time''), a steady-state nucleation regime is reached, corresponding to a steady-state nucleation rate

$$J^{st} = J_0 \exp\left[-\frac{K\sigma^3}{(\ln S_0)^2} \right], \qquad (1)$$

where, for a given temperature, K is a constant which depends on the cluster equilibrium shape and where the prefactor J_0 includes various kinetic parameters. The main predictions of the CTN are in good qualitative agreement with experimental results.[7] Especially, the nucleation rate is found to increase very rapidly with the super-saturation S_0, as expected from Eq. (1). There are still many open questions concerning the validity of this kind of model. However, because it is difficult to perfectly control the experimental conditions and to estimate, for a given system, the various parameters involved in the theory [for instance, in Eq. (1)] it appears quite difficult to perform an experimental quantitative test of the CTN.

The main purposes of this paper are then the following: To propose a numerical test of the CTN, i.e., a direct comparison between the incubation times and nucleation rates predicted by the CTN and those measured in Monte Carlo simulations based on a simple atomistic model. This requires an explicit link between the microscopic parameters involved in the simulations and the macroscopic quantities involved in the CTN.

We also want to show how the details of the diffusion mechanism, which are controlled by the microscopic parameters, can affect the decomposition pathway.

In Sec. II, we will recall the main results of the CTN applied to the case of a binary solid solution and the definition of all the necessary thermodynamic and kinetic parameters. Then a short comparison of these results with a few previous experimental data and numerical simulations is presented. In Sec. III, we describe our Monte Carlo simulations, based on an atomistic kinetic model of diffusion (Sec. III A) and the residence time algorithm (Sec. III B). In Sec. III C we give the sets of microscopic parameters we used, and their link with the data involved in the CTN. The results of Monte Carlo simulations and the comparison with the CTN predictions are given in Sec. IV. After a brief description of a whole nucleation, growth and coarsening sequence (Sec. IV A), we will focus on the steady-state nucleation kinetics (Sec. IV B) and on the transient regime and incubation time (Sec. IV C). In Sec. IV D we show how the details of the atomic diffusion mechanism can modify the kinetic pathway. Section IV E is devoted to the modification of the previous kinetic pathways by addition of impurities. These effects are experimentally well known[8] and Monte Carlo simulations are used to simulate and rationalize such behaviors as the slowing down of the precipitation by vacancy trapping (Sec. IV E 1) or the acceleration of the decomposition by precipitation on nucleation agents (Sec. IV E 2).

II. THE CLASSICAL THEORY OF NUCLEATION

We consider the case of a substitutional A-B alloy with a clustering tendency (i.e., with a phase diagram displaying a

miscibility gap below a critical temperature T_c) and where the diffusion occurs by vacancy jumps. A disordered solid solution of composition C_α^0 is quenched into the miscibility gap, to a temperature T corresponding to the solubility limit $C_\alpha^{eq}(T)$. The first step of the phase separation occurs through thermal fluctuations, which lead to the nucleation of small B-rich clusters of β phase in the α solid solution. The clusters evolution is usually assumed to proceed by evaporation and condensation of B monomers. The evolution of the number $N(i,t)$ of clusters with i B atoms is then given by

$$\frac{dN(i,t)}{dt} = -(\alpha_i+\beta_i)N(i,t)+\beta_{i-1}N(i-1,t) + \alpha_{i+1}N(i+1,t), \quad (2)$$

where α_i and β_i are, respectively, the ''emission'' and ''condensation'' rate for clusters of size i. If these rates are known, the evolution of the cluster size distribution can be computed, starting from any initial distribution $N(i,t=0)$. However, if β_i can be estimated in various physical situations (see below, Sec. III C), such an estimation is much more difficult for the evaporation rate α_i. The classical theory rests on the assumption that α_i is a characteristic of the cluster as defined by its size only. Therefore it can be deduced from a relation of microscopic reversibility such as $\alpha_{i+1}=\beta_i N^{eq}(i)/N^{eq}(i+1)$, derived from the equilibrium situation. The size distribution at equilibrium $N^{eq}(i)$ is then required to compute the evaporation rate. Even with these approximations, an analytical treatment of Eq. (2) remains difficult (especially for the transient regime and the incubation time): a numerical integration is then an alternative tool.[3,9]

The free energy change on forming a β cluster of size i (with a radius R) is given by

$$\Delta F(R) = AR^3\Delta f_v + BR^2\sigma = iV_\beta\Delta f_v + B\left(\frac{iV_\beta}{A}\right)^{2/3}\sigma, \quad (3)$$

where Δf_v is the driving force per unit volume for the precipitation and σ the α/β interfacial energy, V_β is the atomic volume of the β phase, and A and B are some geometric factors (for a spherical cluster $A=4\pi/3$ and $B=4\pi$). For a dilute alloy, it can be shown that in simple cases[1,7]

$$\Delta f_v \simeq -\frac{k_bT}{V_\beta}\ln S_0, \quad (4)$$

where k_b is the Boltzmann constant and $S_0=C_\alpha^0/C_\alpha^{eq}(T)$ the initial supersaturation. For an undersaturated solid solution ($S_0<1$), both terms in Eq. (3) are positive, the solid solution is in a stable equilibrium and is made of solute clusters, the size distribution of which is given by

$$N^{eq}(i) = N_0\exp\left(-\frac{\Delta F(i)}{k_bT}\right), \quad (5)$$

where the appropriate choice for N_0 according to Russell,[5] is the total number of atomic sites rather than the number of B atoms. For a supersaturated solution ($S_0>1$) the first term in Eq. (3) becomes negative. For small clusters, ΔF is positive and increases up to a maximum which defines the critical radius $R^*=-2B\sigma/(3A\Delta f_v)$ and the ''nucleation barrier'' $\Delta F^*=\Delta F(R=R^*)=4B^3\sigma^3/(27A^2\Delta f_v^2)$. The critical clusters of size $R=R^*$ (or $i=i^*$) are in unstable equilibrium with the solid solution: clusters of size $R>R^*$ will grow, while the smaller ones are predicted to redissolve into the solid solution.

A. Steady-state nucleation

The steady-nucleation J^{st} rate is defined as the rate at which subcritical clusters reach the critical size. The first and simplest expression of J^{st} is due to Volmer and Weber who assumed that the critical cluster concentration (in a *metastable* supersaturated solid solution) is still given by the equilibrium distribution [Eq. (5)]. Then

$$J_{VW}^{st} = \beta(i=i^*)N^{eq}(i=i^*) = \beta^*N^*. \quad (6)$$

More sophisticated treatments take into account the possible redissolution of some supercritical clusters and the fact that the equilibrium distribution [Eq. (5)] overestimates the critical cluster concentration.[2–4] They lead to the well-known Becker-Döring expression of the steady-state nucleation rate

$$J_{BD}^{st} = Z\beta^*N^*, \quad (7)$$

where Z is the Zeldovitch factor $Z=[-(\partial^2F/\partial i^2)_{i^*}/(2\pi k_bT)]^{1/2}$.

B. Transient nucleation kinetics: Incubation time

The previous steady-state nucleation rate is reached after a time lag (the so-called incubation time τ_i), which can be interpreted as the time necessary to reach a steady-state concentration of critical clusters, starting from a disordered solid solution.[5] The time dependent nucleation rate is then $J(t)=J^{st}\exp(-\tau_i/t)$. Various theoretical treatments (see Refs. 3 and 9) lead to

$$\tau_i = \frac{1}{\theta\beta^*Z^2} \quad (8)$$

with θ values ranging from 2 for Feder[4] to 4π for Wakeshima.[10] Numerical integrations of the equations (2) usually give a value of τ_i between these two limits (see Refs. 3,9 and Sec. III C).

The previous description and the corresponding expressions of J^{st} and τ_i rely on several assumptions which are highly questionable.[1,6] Let us stress that (i) an essential assumption is that a small (often microscopic) cluster is treated in the same way as a large β phase and described by the same macroscopic thermodynamic parameters such as Δf_v, σ, etc. (ii) Clusters are only defined by the number of monomers they contain, while (especially for small cluster size) various morphologies could be expected. (iii) Growth and decay of the clusters only occur by ''condensation'' and ''evaporation'' of B monomers: possible direct coagulations of small precipitates are not taken into account. A generalization of the CTN, with coagulation and cluster splitting mechanisms, has been proposed by Binder and Mirold,[11] but additional approximations have to be introduced to compute the rates corresponding to these events. (iv) Finally a fundamental approximation is the extrapolation from an equilibrium condition: $\alpha_{i+1}=\beta_iN^{eq}(i)/N^{eq}(i+1)$, at any time, to

compute the emission rate. It corresponds to a situation where the emission is a characteristic of the cluster, but does not depend on the cluster environment.

C. Comparison with experimental results and numerical simulations

Unfortunately, an experimental quantitative test of the CTN is very difficult in the case of solid solutions.[7] The critical size for sufficiently rapid precipitation is indeed generally very small (typically less than 100 atoms), which makes the direct experimental observations of the nucleation stage almost impossible. The quenching conditions are difficult to control : if it is too slow, decomposition can occur during the quench. The vacancy concentration (and so, the diffusion coefficient of B atoms) is rarely known exactly and can evolve after the quench if it is not at its equilibrium value. Moreover, for a given system, the quantities involved in the CTN are often difficult to measure or compute : the interfacial energy, the driving force [which, in addition to the ''chemical'' term of Eq. (4), must take into account the elastic effects], the condensation rate β^*, the solute diffusion coefficient, etc., whereas the predictions of the CTN are very sensitive to small uncertainties on these parameters, especially for those involved in the exponential term of J^{st}. As a result, the uncertainties on the nucleation rates are at least between three and five orders of magnitude [see Refs. 7 and 12 for a discussion of these points, mainly concerning the first and classical experimental test of the CTN, by Servi and Turnbull (1966) who studied the coherent precipitation of cobalt in copper by electrical resistivity measurements[13]].

The experimental situation is often better for non solid systems. The condensation of liquid droplets in a vapor phase is much easier to observe and measure.[14] Unfortunately the free energy formation is much more difficult to calculate for the droplets in a vapor than in condensed phases because of the many degrees of freedom due to the possible translations and rotations. As a consequence, there are commonly uncertainties of at least 10 orders of magnitude on the pre-exponential factor of the nucleation rate.[2]

Because of all the previous difficulties, the use of numerical simulations has been proposed since a long time to test the CTN. The observation difficulties can then be avoided, the aging conditions (vacancy concentrations, temperature, initial configuration, etc.) are perfectly controlled and the use of a simple model avoids additional terms such as those due to elastic effects.

The kinetics of phase separation has been extensively simulated by various Monte Carlo technics (see, e.g., Refs. 1 and 7 for a review). For computational time reasons, however, most of the published studies deal with strongly supersaturated systems and later growth and coarsening regimes rather than with the transient and the steady-state nucleation ones. This later regime has been simulated by Heermann[15] in the case of a two-dimensional ferromagnet under external magnetic field. They checked the exponential dependence of J^{st} as a function of the supersaturation predicted by Eq. (1), with a value of σ close to the estimated one. No estimation of the pre-exponential factor and no observation of the transient kinetics were reported. More recently Shneidman *et al.*[16] observed transient kinetics in the same kind of system and a qualitative agreement between MC and CTN. But he did not achieve a quantitative comparison. Here we consider a solid solution (i.e., a globally conserved instead nonconserved order parameter, diffusion by vacancy jumps rather than Kawazaki mechanism, 3D instead of 2D simulations).

III. MONTE CARLO SIMULATIONS

A. Atomistic kinetic model

We consider a rigid lattice with a body-centered cubic (bcc) structure. The diffusion occurs via vacancy (V) jumps towards nearest-neighbor A or B atoms. The vacancy exchange frequency with, for example, a B atom, is given by

$$\Gamma_{B\text{-}V} = \nu_B \exp\left(-\frac{E_B^{act}}{k_b T}\right), \tag{9}$$

ν_B is an ''attempt frequency'' and the activation energy E_B^{act} is the energy change required to move the B atom from its initial stable position to the saddle point position. E_B^{act} is computed as the difference between the *total* energy of the system when the B atom is in the saddle point position (ε_{SP}) and the *total* energy before the jump (ε_{ini}). Assuming that the energy of the alloy is a sum of pair interactions V_{ij}, it is equal to the binding energy of the B atom at the saddle point (e_s^B) minus the energy of the bonds between the atom and its neighbors before the jump[17]

$$E_B^{act} = \varepsilon_{SP} - \varepsilon_{ini} = e_s^B - \sum_{j \in NN(B)} V_{Bj} \tag{10}$$

For the sake of simplicity, we only consider here the nearest neighbors (NN) of B. E_B^{act} and $\Gamma_{B\text{-}V}$ depend on the local atomic configurations around the B-V pair through the ''broken'' bonds V_{Bj}. In an actual alloy e_s^B can also depend on the atomic configuration around the saddle point position and therefore, it could be computed as a sum of pair interactions between the saddle point atom and its neighbors.[18] However, for the sake of simplicity and since we do not try to fit a specific alloy system, e_s^A and e_s^B (as the attempt frequencies ν_A and ν_B) are assumed to be constant in the following.

B. Monte Carlo methods

This diffusion model can be handled by various kinetic methods, such as mean-field technics[19] or Monte Carlo simulations.[20,21] The latter method is particularly suitable here since it naturally takes into account the correlations between vacancy jumps and the thermal fluctuations, which play a major role in the nucleation process. We use simulation boxes with N_0 lattices sites, N_A A atoms, N_B B atoms, N_V vacancies, and periodic boundary conditions. Typical sizes are $N_0 = 128^3$ atomic sites for a whole precipitation process, $N_0 = 256^3$ for the nucleation rate and incubation time measurements. At each Monte Carlo Step (MCS), a vacancy V can undergo z exchanges with its nearest neighbors (z: coordination number, $z=8$ for the bcc structure), with the corresponding frequencies $\Gamma_1, \Gamma_2, \ldots, \Gamma_z$. One of these exchanges is chosen according to the residence time algorithm (RTA) described elsewhere.[20] It gives an estima-

TABLE I. Microscopic parameters for jump frequencies.

Parameters	Set 1	Set 2
V_{AA}	-1.07 eV	-1.07 eV
V_{BB}	-1.07 eV	-1.24 eV
V_{AB}	-0.985 eV	-1.07 eV
e_s^A	-6.415 eV	-6.5 eV
e_s^B	-6.215 eV	-6.5 eV
ν_A	3.65×10^{15} s^{-1}	1.02×10^{16} s^{-1}
ν_B	3.65×10^{15} s^{-1}	1.02×10^{16} s^{-1}

tion of the physical time associated to each MCS: $t_{\mathrm{MCS}}=(\Sigma_{i=1}^{i=z\times N_{\mathrm{V}}}\Gamma_i)^{-1}$, and is more efficient with the vacancy diffusion mechanism than the Metropolis algorithm, especially at low temperature. As long as vacancy pairs can be ignored, the corresponding physical time scale is inversely proportional to the vacancy concentration C_v in the simulation box. We usually have one vacancy in the simulation box and the times obtained with different box sizes can be directly compared by multiplying $t^*=\Sigma t_{\mathrm{MCS}}$ by the vacancy concentration.

C. Microscopic parameters—Link with the CTN

The precipitation occurs due to vacancy jumps and the kinetics is entirely controlled by (i) the vacancy concentration and (ii) the set of vacancy exchange frequencies with A and B atoms depending on the local atomic configurations. In order to compare the CTN predictions and the Monte Carlo results, the quantities involved in Eqs. (3)–(8) must be related to the microscopic parameters of Eqs. (9),(10). The phase diagram only depends on the mixing energy $\Omega=-(z/2)\times(V_{AA}+V_{BB}-2V_{AB})$. If $\Omega>0$, it displays a miscibility gap below the critical temperature $T_c\simeq0.8\ \Omega/2k_b$ (with the parameters of Table I, $T_c\simeq3155$ K).

Equilibrium shape. For the A and B parameters of Eq. (3), we assume a spherical cluster shape (i.e., $A=4\pi/3$ and $B=4\pi$). Except for very small sizes, this is indeed the shape observed in the simulations at relatively high temperatures (for approximately $T>T_c/2$). When the temperature decreases, interfaces become planar with a faceting by {110} crystallographic planes. Stable clusters tend to adopt a regular dodecahedron shape,[20] sufficiently close to the spherical one to keep the same value for A and B.

Driving force. In our case (simple unmixing and dilute solution) the driving force for precipitation [Eq. (4) with $V_\beta=a^3/2$] is related to the solubility limit (via the supersaturation $S_0=C_\alpha^0/C_\alpha^{\mathrm{eq}}$) which at low temperature ($T\leqslant0.3\times T_c$) is correctly given by the well-known mean-field (Bragg-Williams) approximation. At higher temperature this approximation becomes too poor and the actual solubility limit is carefully determined by a standard semi grand-canonical Monte Carlo simulation.[22,23]

Interfacial energy. Within the conditions we study (low supersaturations, temperatures far from the critical one), the precipitate interface remains sharp, with a typical width close to the lattice parameter a. According to Becker's theory, the α/β interfacial energy σ can be related to the mixing energy by counting the number of ''wrong'' A-B bonds by area unit[5]

$$\sigma_{\langle hkl\rangle}=\frac{\varepsilon_{\langle hkl\rangle}\Omega}{a^2}(C_\alpha^{eq}-C_\beta^{eq})^2 \tag{11}$$

where $\varepsilon_{\langle hkl\rangle}$ is a geometric constant which depends on the interface crystallographic orientation $\langle hkl\rangle$. For the numerical results we use a typical value of $a=0.287$ nm (that of the bcc iron). For higher temperatures and supersaturations, a diffuse interface model would have to be considered, with σ computed according to the Cahn-Hilliard method,[24] Monte Carlo,[25,26] cluster variation[25] or low-temperature expansion[27] methods.

Condensation rate. The expression for the condensation rate β^* of a B atom on a critical cluster depends on the limiting step.[1] If the condensation is limited by the jump of B across the interface, β^* is proportional to the cluster area $\beta^*\propto2\pi(R^*)^2\Gamma_{B\text{-}V}C_\alpha^0/a^2$. In our case, the adsorption is clearly limited by the long-range diffusion of B towards the matrix. By solving the corresponding diffusion equation one gets[1,6]

$$\beta^*=8\pi R^* D_B^\alpha C_\alpha^0/a^3, \tag{12}$$

where D_B^α is the diffusion coefficient of B in the α matrix. The two previous expressions for β^* are indeed numerically rather close as far as the critical radius does not exceed a few lattice parameters. D_B^α is a key parameter and must be carefully estimated in order to take into account the effect of the vacancy mechanism, i.e., correlation between successive vacancy jumps. The expression of D_B^α as a function of the various B jump frequencies is provided by the theory of diffusion in dilute alloys (see the Appendix). It strongly depends on the set of microscopic parameters.

Asymmetry effects on the diffusion mechanism: migration of B monomers and small clusters. Indeed, it must be emphasized that two sets of microscopic parameters $\{V_{AA},V_{BB},V_{AB},e_s^A,e_s^B,\nu_{A,},\nu_B\}$ can give the same mixing energy (i.e., the same equilibrium phase diagram and the same interfacial free energy σ) and the same D_B^α for B monomers, while the details of the diffusion mechanism of B are different. That means that they will give different kinetic pathways, especially different nucleation rates and incubation times, even if the classical predictions of Eqs. (7) and (8) are the same.

Such differences come from the ''asymmetry effects,'' extensively studied by Athènes *et al.*,[21] which reflect the tendency of a vacancy to exchange rather with A or B atoms. In our diffusion model two degrees of asymmetry can be defined $a^*=(V_{AA}-V_{BB})/(V_{AA}+V_{BB}-2V_{AB})$ and $c^*=e_s^A-e_s^B$. An important result is that the relative mobility of B monomers and small B clusters (dimers, trimers, etc.) strongly depends on the value of a^* and c^*.[21,28]

In the following, we use two sets of parameters (Table I). They correspond to the same values of all the quantities involved in the CTN (especially D_B^α, see the Appendix). With the second one ($a^*=-1$ and $c^*=0$), as we will see later and as it can be expected from Athènes' results,[21] only B monomers are mobiles. With the first one ($a^*=0$ and $c^*<0$), small B clusters can migrate too: it comes mainly from the fact that in this case, the vacancy is trapped on B monomers and small clusters. For this reason, the first set of pa-

rameters is less time consuming and it has been used more extensively in our simulations. However the simulations performed with the second set of parameters are closer to the CTN situation: when only B monomers can migrate, one can expect that β clusters will evolve only by evaporation and condensation of individual B atoms.

IV. RESULTS AND DISCUSSIONS

Precipitation processes will be studied in Monte Carlo simulations starting from completely disordered (random) solid solutions, at various temperatures and supersaturations. For the first time (Secs. IV A–IV C) the first set of parameters of Table I will be used. A β cluster is defined as a set of B atoms, each of which is a nearest neighbor of at least one B atom in that cluster. Once the critical size i^* has been determined, the evolution of the number $N_p(i>i^*)$ of supercritical β clusters and their average size $\langle i\rangle$ (in number of B atoms in the cluster) are directly measured. Unfortunately, it is very difficult to get i^* directly from the observation of the cluster size distribution, since no discontinuities are expected at the critical size.[2,7] It is then estimated from the minimum of Eq. (5). We will see in Sec. IV B that the equilibrium distribution predicted by Eq. (5) is relatively well checked during the nucleation stage: this point tends to justify the use of the classical value for i^*.

A. General kinetic evolution: Nucleation-growth-coarsening

Figure 1 gives an example of a whole precipitation sequence, with the first set of parameters of Table I, at $T=0.4\ \Omega/2k_b$ ($\simeq 0.5\ T_c$) and at a relatively small supersaturation ($C_\alpha^0=3\%$, i.e., $S_0\simeq 3.75$). The simulation box contains $N_0=128^3$ lattice sites. As can be seen, the classical picture holds quite well. One observes the four classical stages: incubation (approximately for $t^*\times C_v<5\times10^{-13}$ s); nucleation (for 5×10^{-13} s$<t^*\times C_v<10^{-11}$ s) during which the number of precipitates N_p increases linearly with the time, while their size $\langle i\rangle$ is approximately constant; growth (for 10^{-11} s$<t^*\times C_v<2\times10^{-10}$ s) during which a sudden drop of the supersaturation leads to a rapid increase of the precipitate size: $\langle i\rangle \propto t^\alpha$ (with the classical growth $\alpha=3/2$ value, i.e., $R\propto t^{1/2}$) while their number evolves slowly; and finally, after a transient regime, the coarsening (for $t^*\times C_v>10^{-9}$ s): the matrix has almost reached its equilibrium composition, the smallest precipitates shrink to the benefit of the larger ones and one observes the classical exponents: $\langle i\rangle\propto t$ (i.e., $R\propto t^{1/3}$) and $N_p\propto t^{-1}$. It has been observed that the growth regime vanishes as the initial supersaturation increases: the exponent α decreases and the bump on the $\langle i\rangle$ versus t curve flattens. This can be explained by the contribution of small clusters direct coagulation to the precipitation. For the same reason, α is also sensitive to the asymmetry of diffusion. These effects are discussed by Athènes *et al.* in Ref. 21. We will now focus on the first steps of the precipitation.

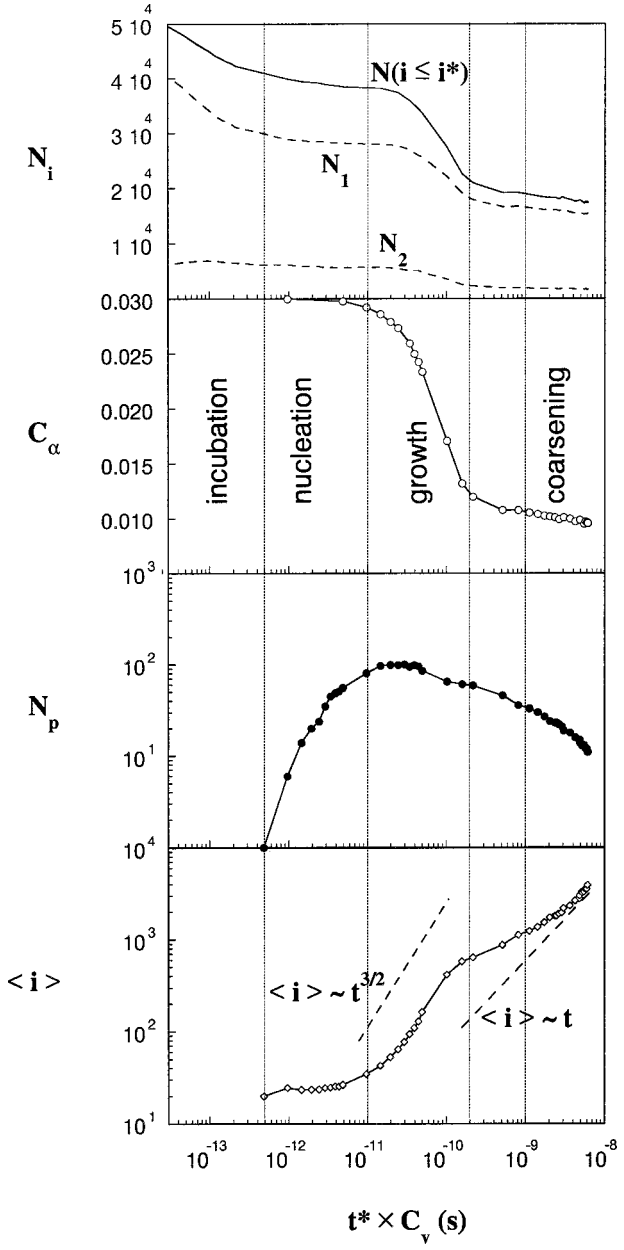

FIG. 1. Decomposition of a metastable solid solution of composition $C_\alpha^0=3\%$ during a thermal aging at $T=0.4\ \Omega/2k_b$ (i.e., $T\simeq 0.5T_c$ and $S_0\simeq 3.75$). The critical size is $i^*=19$ atoms. From the top to the bottom: evolution of the total number of subcritical clusters [$N(i\leqslant i^*)$, full line], together with the number of B monomers and dimers (N_1 and N_2, dotted lines); of the α matrix composition C_α (○); of the total number of supercritical clusters $N_p(i>i^*)$ (●) and of the averaged cluster size $\langle i\rangle$ (◇). Monte Carlo simulations with the first set of parameters of Table I, 128^3 lattice sites and 1 vacancy.

B. Nucleation rate

At supersaturations lower than the one of Fig. 1, the critical size increases and so the supercritical cluster density decreases very rapidly. It is then necessary to use larger simulation boxes ($N_0=256^3$ lattice sites) to observe a sufficient number of supercritical clusters in a reasonable computational time, and therefore to be able to measure nucleation rates and incubation times with a sufficient precision. Depending on the supersaturation, two kinds of behaviors can be observed. At low supersaturation [e.g., $S_0\simeq 3.75$, as shown in Fig. 2(a)], the evolution of the number of supercritical clusters clearly displays an incubation time, then a steady-state nucleation rate which can be directly measured.

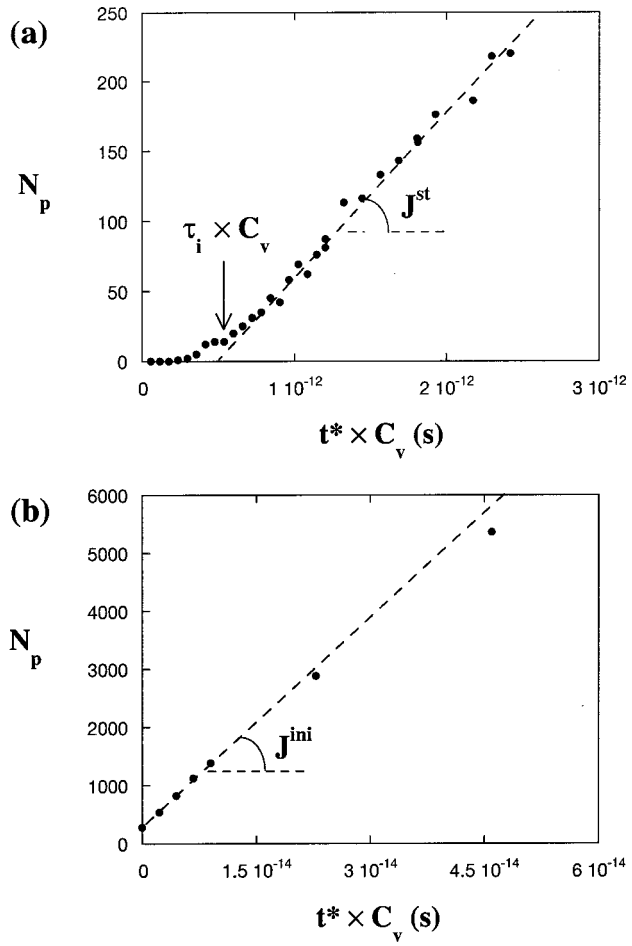

FIG. 2. Evolution of the number of supercritical clusters N_p at the beginning of the precipitation process (nucleation). Monte Carlo simulations with the first set of parameters of Table I, 256^3 lattice sites and 1 vacancy. (a) For $T=0.4\ \Omega/2k_b$ and $C_\alpha^0=3\%$ (i.e., $T\simeq 0.5T_c$ and $S_0\simeq 3.75$), (b) for $T=0.4\ \Omega/2k_b$ and $C_\alpha^0=6\%$ (i.e., $T\simeq 0.5T_c$ and $S_0\simeq 7.5$).

At higher supersaturation [e.g., $S_0\simeq 7.5$, Fig. 2(b)], the incubation time vanishes and no steady-state nucleation rate can be defined. However, an initial nucleation rate $J^{\rm ini}$ can still be measured at $t=0$ [dotted line on Fig. 2(b)].

1. Cluster size distributions

During the steady-state nucleation regime, when it occurs, the observed cluster size distribution can be compared to that predicted by Eq. (5). As can be seen in Fig. 3, the agreement is reasonable: the use of the classical expression to determine the critical size is then justified. As expected, the equilibrium expression overestimates the critical cluster concentration, a fact which is taken into account in Eq. (7) by the Zeldovitch factor.

However some differences between simulated and classical distributions can be observed, especially for very small cluster sizes. This is not surprising, because of the uncertainties on the quantities involved in Eq. (3), the assumption on the (spherical) cluster shape and the lack of line and point contributions which, in addition to the bulk and surface terms of Eq. (3), should be taken into account in the free energy of small clusters, as shown by Perini *et al.*[26]

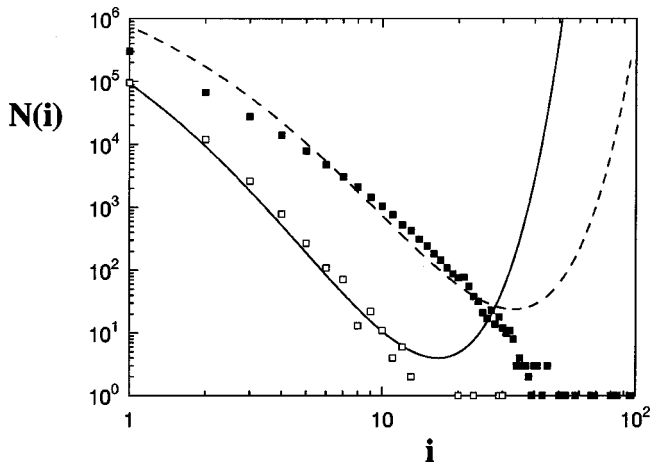

FIG. 3. Cluster size distribution during the steady-state nucleation stage. The lines correspond to the equilibrium distribution of Eq. (5), the squares to the Monte Carlo simulations (with the first set of parameters of Table I, 256^3 lattice sites, 1 vacancy). Full squares, dotted line: $T=0.5\ \Omega/2k_b$ and $C_\alpha^0=4.5\%$ (i.e., $T\simeq 0.625T_c$ and $S_0\simeq 2.25$); empty squares, full line: $T=0.2\ \Omega/2k_b$ and $C_\alpha^0=0.8\%$ (i.e., $T\simeq 0.25T_c$ and $S_0\simeq 6.3$).

2. Evolution of the nucleation rate with the supersaturation

The evolution of $J^{\rm st}$ (or of $J^{\rm ini}$ for the higher supersaturations) is represented as a function of S_0 on Fig. 4 for various temperatures. As expected from the CTN equations (4)–(7), the exponential of $J^{\rm st}$ is found to decrease as $(\ln S_0)^{-2}$, with a slope which gives an interfacial energy σ very close to the $\sigma_{\langle 110\rangle}=460\ {\rm mJ\,m^{-2}}$ value estimated at low temperature from the interactions potentials of Table I, according to Eq. (11) (the $\langle 110\rangle$ interfaces being that of lowest energy). It must be noticed that indeed the agreement is still valid at

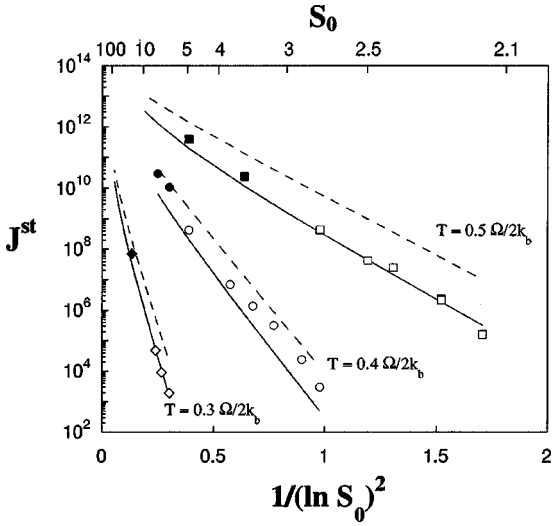

FIG. 4. Evolution of the steady-state nucleation rate $J^{\rm st}$ with the supersaturation. Monte Carlo simulations at $T=0.3\ \Omega/2k_b$ ($\diamond$), $T=0.4\ \Omega/2k_b$ ($\circ$), and $T=0.5\ \Omega/2k_b$ ($\square$) (first set of parameters of Table I, 256^3 lattice sites, 1 vacancy). The black symbols for high super-saturations correspond to initial nucleation rates $J^{\rm ini}$ in the case where no steady state is reached. Classical theory: Volmer-Weber [Eq. (6), dotted line] and Becker-Döring [Eq. (7), full line] estimations.

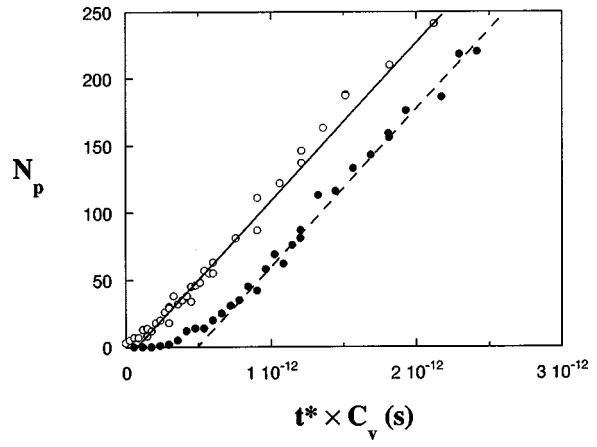

FIG. 5. Evolution of the number of supercritical clusters N_p at the beginning of the precipitation process at $T=0.4\ \Omega/2k_b$ and $C_\alpha^0=3\%$ (i.e., $T\simeq 0.5T_c$ and $S_0\simeq 3.75$): (●) starting from a random solid solution and (○) starting from a solid solution maintained during 2×10^9 MCS just above the solubility limit (at $T=0.55\ \Omega/2k_b\simeq 0.69T_c$). Monte Carlo simulations with the first set of parameters of Table I, 256^3 lattice sites and 1 vacancy.

high supersaturation where no steady state is reached (this is the case for the few black symbols on Fig. 4). In view of the great sensitivity of J^{st} on small uncertainties on σ, the clusters shape and β^*, the CTN prefactor is also in good agreement with the Monte Carlo simulation. Moreover, in most cases, the predictions of the Becker-Döring theory [Eq. (7)] are closer to the Monte Carlo results than those of the simpler Volmer-Weber theory [Eq. (6)].

C. Incubation time

The terminology concerning the incubation concept is indeed often confusing. In the CTN, the incubation time (sometimes called time-lag or induction time) is defined as the time necessary to obtain the metastable equilibrium concentration of critical clusters, starting from a random solid solution. In experiments, the ''incubation time'' often refers to the time necessary to observe the first precipitates: it clearly depends on the experimental resolution. In Monte Carlo simulations, as can be seen from Fig. 2(a), starting from a completely random solid solution, one has to wait for a time τ_i before to reach a steady-state nucleation regime. This later time τ_i corresponds to the classical concept of incubation and will be compared in the following to the classical predictions.

This can be illustrated by the following simulation (Fig. 5): prior to the quench at the decomposition temperature T, the system is maintained for a long time at a temperature $T+\Delta T$ just above the miscibility gap. The under-saturated solid solution reaches a *stable* equilibrium state, i.e., the equilibrium cluster size distribution and the equilibrium value of the short range order parameter. If the system is then quenched to T (at time $t=0$) the solid solution decomposes, but starting from a state which is quite close to its new *metastable* equilibrium state, rather than from a random configuration: if ΔT is not too high, the incubation period vanishes.

On the other hand, after the incubation regime, once the steady state has been reached, the mean time necessary to observe the nucleation of a new stable cluster in a system of

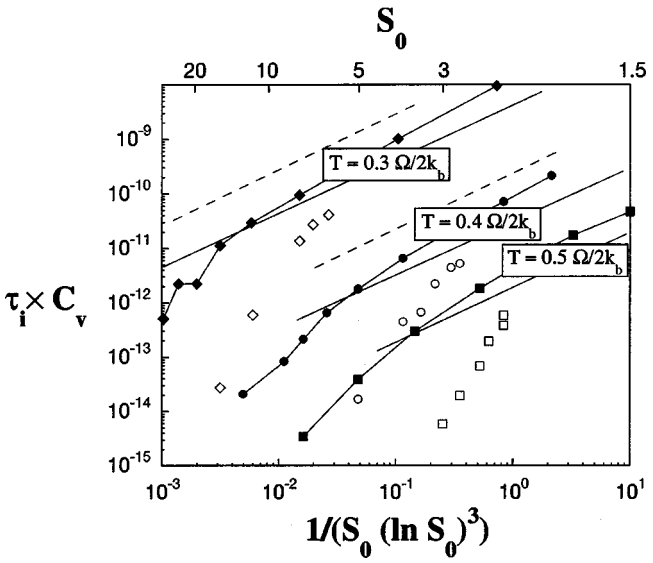

FIG. 6. Evolution of the incubation time with the supersaturation. Monte Carlo simulations at $T=0.3\ \Omega/2k_b$ (◇), $T=0.4\ \Omega/2k_b$ (○), and $T=0.5\ \Omega/2k_b$ (□) (first set of parameters of Table I, 256^3 lattice sites, 1 vacancy). Classical theory: numerical integration of Eq. (2) at $T=0.3\ \Omega/2k_b$ (◆), $T=0.4\ \Omega/2k_b$ (●), and $T=0.5\ \Omega/2k_b$ (■), and Feder's [$\tau_i=1/(2\beta^*Z^2)$, dotted line] and Wakeshima's [$\tau_i=1/(4\pi\beta^*Z^2)$, full line] estimations. For the sake of clarity, Feder's estimation has been omitted for $T=0.5\ \Omega/2k_b$.

volume V will be $\tau_n=1/(V\times J^{st})$. Notice that τ_n depends on the size of the system, while τ_i does not. Moreover at a given temperature, $\tau_n\propto\exp(\ln S_0)^{-2}$ evolves more rapidly with the supersaturation than $\tau_i\propto 1/[S_0\times(\ln S_0)^3]$. A third time is sometimes introduced for finite-size systems: $\tau_1=\tau_i+\tau_n$ is the time of apparition of the first supercritical cluster.[16]

Figure 6 displays the incubation times τ_i measured in the simulations performed with the first set of parameters of Table I for three temperatures. It is compared with three estimations of the ''classical'' incubation time: two analytical expressions of Feder [$\tau_i=1/(2\beta^*Z^2)$] and Wakeshima [$\tau_i=1/(4\pi\beta^*Z^2)$] and one obtained by numerical integration of Eq. (2). All these estimations predict that the incubation time decreases with increasing supersaturation as $1/[S_0\times(\ln S_0)^3]$ (the exact dependence of τ_i with S_0 depends on the approximation chosen for β^*). As can be seen, strong and weak supersaturations have to be distinguished.

For small supersaturations the order of magnitude is reasonable, even if incubation time measured in the simulations is lower than the estimated one. As it has been already observed,[3,9] numerical integration of cluster dynamic Eq. (2) gives, for small supersaturations, incubation times between Feder's and Wakeshima's estimations. In the simulations τ_i is found to be smaller than predicted by the Feder's expression and closer, but still lower than the Wakeshima's prediction. Simulations at lower supersaturations would of course be very useful for a more quantitative comparison. Unfortunately, such conditions correspond to larger critical nucleus and longer incubation times and they would require too large simulation boxes and too long simulation times.

As we will see in the next section, the origin of a large part of the discrepancy can be the contribution, in addition with individual B atoms, of small β clusters which can mi-

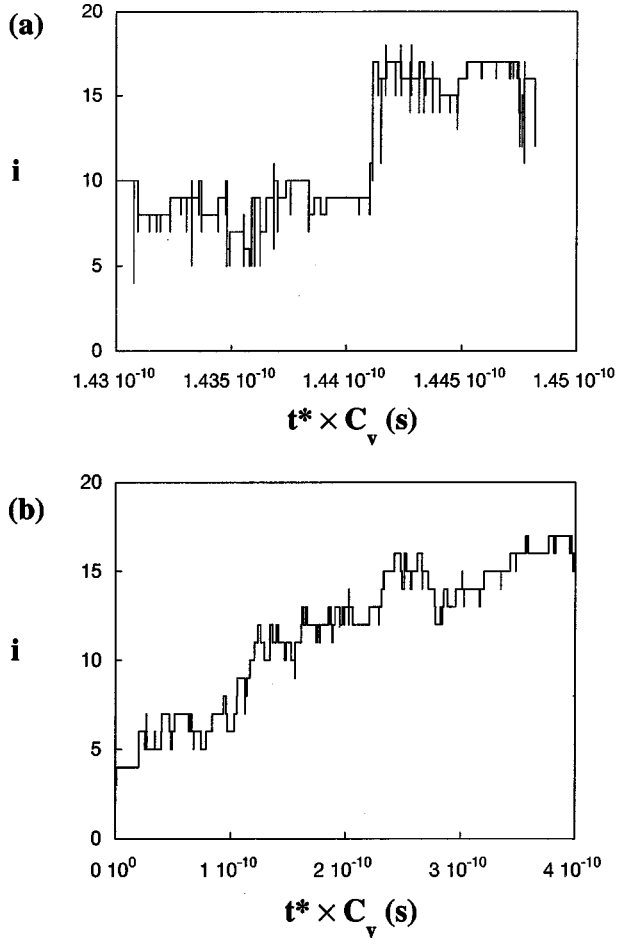

FIG. 7. Time evolution of the size of one β cluster at $T=0.3\ \Omega/2k_b$ and $C_\alpha^0=1\%$ ($T\simeq 0.375\ T_c$ and $S_0\simeq 7.7$). Monte Carlo simulation with 32^3 lattice sites, 1 vacancy and: (a) the first set of parameters of Table I, (b) the second set of parameters of Table I.

grate and directly coagulate with other clusters, and thus accelerate the nucleation process.

For high supersaturations, the incubation time measured in the simulations drops much more rapidly than expected from the classical theory. It must be noticed that even for the highest supersaturations used in the simulations corresponding to Fig. 6, the nucleation barrier is still much higher than k_bT (with typically $\Delta F^*>6\ k_bT$), so that the CTN should be valid.[1,7] However, the incubation time measured in the simulations can be two orders of magnitude smaller than predicted. Once again, the contribution of direct coagulation of small β clusters can explain a part of this discrepancy, but only a part of it, as will be seen in the next section.

D. Effects of diffusion mechanisms on nucleation kinetics

All the previous results have been obtained with the first set of parameters of Table I, i.e., in a case where both *B* monomers and small *B* clusters can migrate. One can expect that the contribution of these latter clusters (which is not taken into account in the classical expression of τ_i and J^{st}) leads to a general acceleration of the nucleation processes. With the second set of parameters, only the *B* monomers can migrate, all the quantities involved in the CTN (especially

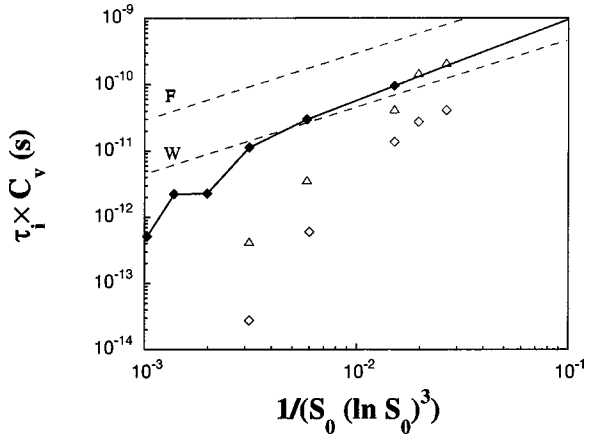

FIG. 8. Evolution of the incubation time as a function of the supersaturation. Monte Carlo simulations with the first (◇) and the second (△) set of parameters of Table I, 256^3 lattice sites, 1 vacancy. Classical theory: Wakeshima's (dotted line, *W*) and Feder's (dotted line, *F*) estimations; numerical integration of Eq. (2) (full line, ◆).

D_B^α, see the Appendix) remaining the same as with the previous set of microscopic parameters.

At a microscopic scale, the effect of the small *B* clusters mobility is illustrated on Fig. 7, which shows the evolution of the number of *B* atoms in *one* given β cluster during simulations at $T=0.3\ \Omega/2k_b$ and $C_\alpha^0=1\%$ (i.e., $T\simeq 0.375\ T_c$ and $S_0\simeq 7.7$) performed using the two sets of parameters of Table I. In the first case [Fig. 7(a)], the cluster can suddenly undergo a growth or decay of $\pm 3,4,\ldots$, or even 7 *B* atoms because clusters of such sizes can migrate in the matrix. In the second case [Fig. 7(b)], the cluster size evolves only by ± 1 steps which correspond to the evaporation and condensation of individual *B* atoms.

The effect on the incubation time and nucleation rate is illustrated on Figs. 8 and 9. When small *B* clusters can migrate the incubation time is smaller and the nucleation rate is larger than when only *B* monomers are mobile. At $T=0.3\ \Omega/2k_b$, the difference can reach almost one order of

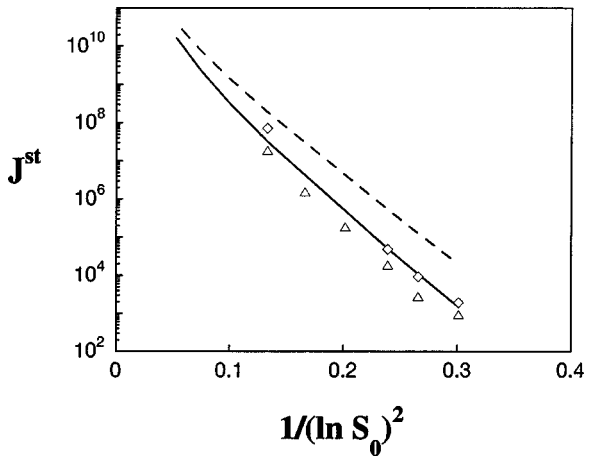

FIG. 9. Evolution of the nucleation rate as a function of the supersaturation. Monte Carlo simulations with the first (◇) and the second (△) set of parameters of Table I, 256^3 lattice sites, 1 vacancy. Classical theory: Volmer-Weber [Eq. (6), full line] and Becker-Döring estimations [Eq. (7), dotted line].

magnitude for the incubation time (Fig. 8) and a factor 3 for the nucleation rate (Fig. 9). The difference must even be higher at lower temperature (since correlation effects increase). For low supersaturations, when diffusion occurs only by migration of B monomers, the incubation time is between Feder's and Wakeshima's estimations, and it becomes very close to the value obtained by numerical integration of Eq. (2). As it could be expected, since the contribution of the direct coagulation of small clusters is not taken into account in the CTN, the Monte Carlo results are closer to the classical prediction with the second set of parameters.

However, as can be seen on Fig. 8, this cannot explain all the discrepancy with the classical expression of τ_i for high supersaturations. A part of the remaining difference must indeed be due to the fact that the value of β^* given by Eq. (12) is underestimated at high supersaturation, when the critical clusters becomes very small (typically $i^*<20$). They have then more complex shapes than spherical ones[20] and their corresponding surface-to-volume ratio is larger. As an example, for the highest supersaturation used in the simulations of Fig. 8 ($S_0 \simeq 15$), the critical size is indeed very small ($i^* \simeq 5$) and a direct examination of the microstructure during the nucleation stage suggests a surface-to-volume ratio of critical clusters approximately 3 times larger than the one given by the spherical approximation used to get Eq. (12). Moreover, one observes for such cases important time fluctuations of the clusters interface.[29] For $i^*<20$, the order of magnitude of these fluctuations can be of the size of the critical cluster itself. The assumption of a spherical and static critical cluster then leads to an underestimation of β^*.

Vacancy versus direct-exchange mechanisms. A related important issue is the comparison with Monte Carlo simulations based on Kawazaki dynamics (i.e., direct exchange mechanism between neighboring atoms), which are commonly used to study phase separation or ordering. Several authors[21,30] have studied to what extent the Kawazaki mechanism affects the kinetic pathway, as compared with the more realistic vacancy exchange mechanism. They suggested, for instance, that the classical Lifshitz-Slyosov-Wagner (LSW) coarsening regime ($R \propto t^{1/3}$) is reached faster with the vacancy mechanism. It has also been claimed that direct exchange favors the coarsening by monomers evaporation-condensation while vacancy exchange favors direct coagulation.

However, we have seen here that the vacancy diffusion mechanism yields these various behaviors, depending on the choice of the microscopic parameters which control the asymmetry in diffusion properties of A and B atoms. In an extensive study on this topic, Athènes *et al.*[21] have shown that most of these various kinetic pathways can be reproduced by a suitable choice of the parameters of a direct-exchange mechanism, provided that the exchange activation energies are computed as a difference between the saddle-point and the initial energy of the system $E^{\mathrm{act}}=\varepsilon_{\mathrm{SP}}-\varepsilon_{\mathrm{ini}}$, and not as the difference (or a fraction of the difference) between the configurational energies before and after the exchange $E^{\mathrm{act}}=\varepsilon_{\mathrm{fin}}-\varepsilon_{\mathrm{ini}}$, as it is done in the classical kinetic Ising model (see Sec. III A). However, the direct exchange mechanism cannot fully reproduce the kinetic pathways which imply the segregation of vacancies at precipitate-matrix interfaces, in particular the latter increase of the contribution of direct coagulation to the coarsening process at low temperature.

Elastic effects. One of the limitations of these simulations is that elastic strains, which are present in many alloy systems, are not taken into account. Such effects mainly result in a reduction of the total driving force. In the frame of the CTN, it can be simply taken into account by the addition of an elastic contribution to the chemical term of Eq. (3) and leads to a general slowing down of the decomposition. It is also well known that the equilibrium shape of the coherent β precipitates depends on their size.[31] Phase field methods (see, e.g., many examples in Ref. 32) and Monte Carlo simulations (with direct exchange mechanisms[33–35]) have been proposed to study such effects (but to our knowledge, they have not been used to address the question of incubation).

Beyond these classical effects, one may speculate that the details of the diffusion mechanisms, for example, the relative mobility of monomers and small clusters would be affected by elastic strains, but that the kinetic pathway would still be dictated by the mobility spectrum of various β clusters. However, for the time being, even for fully coherent phase transformations, the introduction of strain interactions using more realistic (e.g., embedded atom method) potentials would considerably increase the computer time since long range interactions would have to be computed (including in the saddle point positions) at each vacancy jump. Monte Carlo simulations would then become very time consuming, at least for the kind of systems we study here (i.e., large systems, at low concentrations and low temperatures, with strong correlations effects).

E. Impurity effects

For a given supersaturation and temperature, the kinetics of precipitation in a binary A-B alloy will occur according to the behaviors described above. However, for practical reasons, it can be very useful to modify and control this process, for example to avoid or to stabilize a given microstructure. In many industrial metallurgical processes, this is achieved by addition of a third C element.[8] In this section, we show how our simulation method can be used to predict and rationalize some of these impurity effects.

1. Vacancy trapping

A first and very simple effect is the vacancy trapping by the C impurity. If the vacancies spend a constant ratio of their time on immobile C atoms, and if these ''trapped'' vacancies are not replaced in the α matrix (because they are not equilibrium but quenched-in vacancies, or because the kinetics of precipitation are too quick to allow the point defect sources to supply new vacancies), the whole precipitation process will be slowed down by the same ratio. Such a trapping occurs when the formation energy of vacancies is significantly lower near C atoms than on the other atomic sites (in pure A). In our atomistic model, the difference on formation energy between atomic sites nearest neighbor of a C atom and atomic sites in pure A is $\Delta E_v^{\mathrm{for}}=V_{AA}-V_{AC}$, i.e., the vacancy trapping effect becomes important if $V_{AC} \gg V_{AA}$. One can take for example the case of large C atoms on a A-B lattice with a small lattice parameter, which will

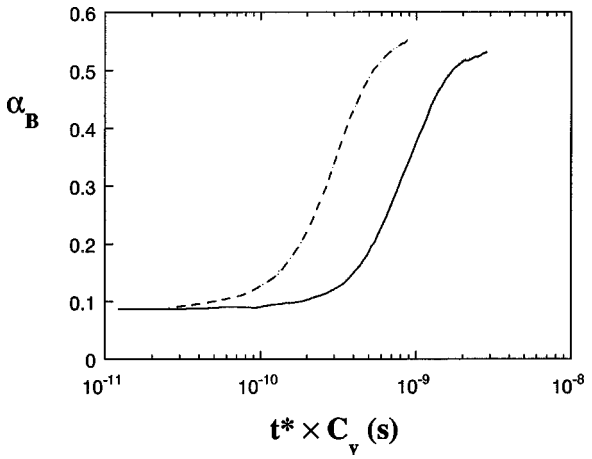

FIG. 10. Evolution of the Warren-Cowley parameter of B atoms at $T=0.4\ \Omega/2k_b$ in a $A_{97.5}B_{2.5}$ alloy ($T\simeq 0.5T_c$ and $S_0\simeq 3$) with (full line) and without (dotted line) an addition of 10 ppm of vacancy trapping impurities (see text). Monte Carlo simulations with the first set of parameters of Table I, 128^3 lattice sites, 1 vacancy.

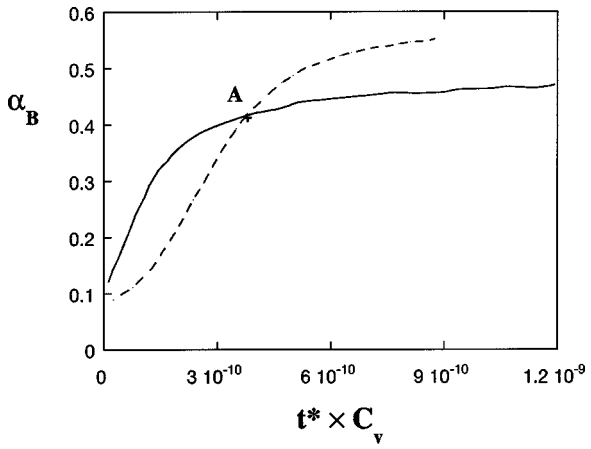

FIG. 11. Evolution of the Warren-Cowley parameter of B atoms at $T=0.4\ \Omega/2k_b$ in a $A_{97.5}B_{2.5}$ alloy with (full line) and without (dotted line) an addition of 100 ppm of clusters stabilizing impurities (see text). Monte Carlo simulations with the first set of parameters of Table I, 128^3 lattice sites, 1 vacancy.

have high and positive interactions energies in stable (V_{AC}, V_{BC}, V_{CC}) as in saddle point (e_s^C) positions.

Figure 10 illustrates such a slowing down of the β precipitation in a $A_{97.5}B_{2.5}$ alloy, with the first set of parameters of Table I, at $T=0.4\ \Omega/2k_b$ ($\simeq 0.5T_c$). It displays the evolution of the Warren-Cowley parameter α_B (which characterizes the B atomic fraction around B atoms, i.e., the B short range order), a convenient way to follow the whole precipitation process.

The dotted line corresponds to the precipitation kinetics without C addition. α_B is found to follow a Johnson-Mehl-Avrami law $\alpha_B=\alpha_B^{\infty}\{1-\exp(-kt^n)\}$.[20] The full line corresponds to the precipitation kinetics with an addition of N_C atoms (corresponding to 10 ppm) with $V_{AC}=+0.3$ eV (and $V_{BC}=+0.3$ eV, $V_{CC}=+2$ eV, $e_s^C=+3.5$ eV). At this temperature, the vacancy spends approximately $z\times(N_C/N_0)\times\exp(-\Delta E_v^{\text{for}}/k_bT)\simeq 2$ more times on nearest-neighbor positions of C atoms than on the other lattice sites and, as can be seen on Fig. 10, the whole precipitation kinetics is simply slowed down by a constant ratio (approximately a factor of 3). At lower temperatures, the trapping effect becomes rapidly much more important and can completely ''freeze'' the kinetics.

It should be noticed that the trapping ratio depends only on $V_{AA}-V_{AC}$. The other C parameters (i.e., mainly the e_s^C energy for small C contents) will only affect the correlation between successive V-C exchanges, not the vacancy concentration around C atoms. With lower (even negative) values of V_{BC}, V_{CC}, and e_s^C, the same slowing down rate will be obtained resulting from a great number of very rapid V-C exchanges rather than from a smaller number of slower exchanges.

2. Stabilization of small clusters

An opposite effect is obtained by adding an impurity C which will stabilize small β clusters. A small number of C atoms with a high ordering tendency with B atoms in the α solid solution (i.e., such as $V_{BC}\ll V_{AB}$ and V_{AA}) will form very stable clusters of B atoms nearest-neighbor of a C atom, for size ($i\sim 8$) which can be far below the critical one.

As in Fig. 10, the dotted line of Fig. 11 corresponds to the time evolution of α_B in a binary $A_{97.5}B_{2.5}$ alloy at $T=0.4\ \Omega/2k_b$. The full line gives the kinetics with an addition of 100 ppm of C atoms such as $V_{BC}=-2.0$ eV (and $V_{AC}=-1.07$ eV, $V_{CC}=-1.07$ eV, $e_s^C=e_s^A=-6.415$ eV: the C atoms have the same properties as the A ones except for their interaction with B atoms). As expected, due to the strong B-C interactions, small B clusters are stabilized for $i\sim 8$, while the critical size without C atoms, for this supersaturation and temperature, is $i^*\simeq 30$ atoms. As a result, the incubation and nucleation stages are almost skipped and the growth regime occurs much more rapidly: the beginning of the precipitation process is greatly enhanced. However, at the end of the growth regime, the microstructure presents a higher density of smaller stable β clusters than without C atoms. The late coarsening stage (for approximately $t^*\times C_v>5\times 10^{-10}$ s) is then slowed down. This situation is illustrated on Fig. 12, which displays the microstructures observed with and without C impurities near the end of the growth stage, at a time corresponding to the crossover point of Fig. 11, i.e., to the same average short range order (approximately $\alpha_B\simeq 0.42$).

V. CONCLUSION

The decomposition of an A-B metastable (A-rich) solid solution, where diffusion occurs by vacancy jumps, is studied by Monte Carlo simulations. A link is established between the microscopic parameters which enter the jump frequencies of the simulations and the thermodynamic and kinetic quantities involved in the classical theory of nucleation. The nucleation rates and incubation times predicted by the CTN can then be compared to those measured in the simulation, with uncertainties of approximately one order of magnitude and without any adjustable parameter. Although it relies on several crude approximations, CTN predictions is in good general agreement with the simulations, for weakly supersaturated solutions and when diffusion occurs only by

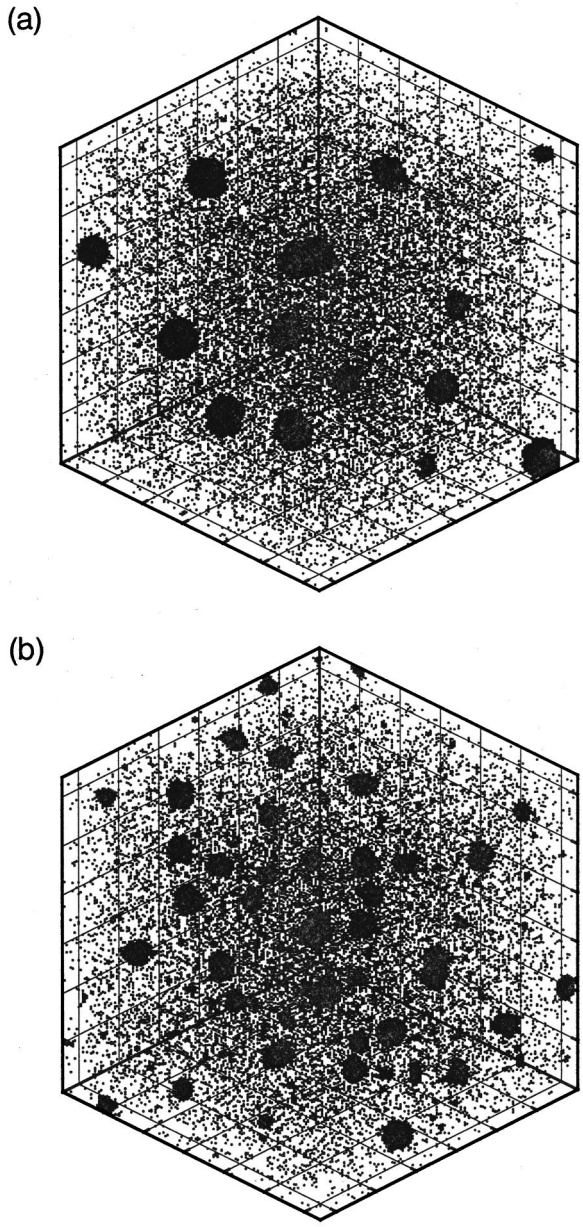

FIG. 12. Microstructure of an $A_{97.5}B_{2.5}$ alloy (a) without and (b) with an addition of 10 ppm of nucleating impurities (see text) after an aging of $t^* \times C_v \sim 3.75 \times 10^{-10}$ s at $T=0.4\ \Omega/2k_b$ (this time corresponds to the crossover point *A* on Fig. 11). Only *B* atoms are represented. Monte Carlo simulations with the first set of parameters of Table I, 128^3 lattice sites, 1 vacancy.

migration of *B* monomers. The nucleation rate and incubation times have approximately the good evolution as a function of the supersaturation and the good orders of magnitude. However, at higher supersaturations the incubation time measured in the Monte Carlo simulations decreases much more rapidly than predicted by the CTN, despite the fact that we are still in a nucleation regime (i.e., with $\Delta F^* \gg k_b T$).

The relative mobility of *B* monomers and small *B* clusters can be controlled by an appropriate choice of the microscopic parameters: when small *B* clusters become mobile, the direct coagulation between small precipitates leads to a general acceleration of the precipitation, i.e., to an increase of the nucleation rate and a decrease of the incubation time (e.g., by one order of magnitude at $T=0.3\ \Omega/2k_b \simeq 0.375 T_c$).

The addition of a third *C* element can also be used to modify the kinetic pathways. Two kinds of such effects have been investigated with the Monte Carlo simulations: a ''vacancy trapping'' effect which produces a general slowing down of the decomposition and a stabilization of subcritical clusters by the *C* impurities, which leads to an acceleration of the nucleation and growth regimes, but to a slowing down of the late-stage coarsening.

ACKNOWLEDGMENTS

Useful discussions with Manuel Athènes are gratefully acknowledged. We thank Bernard Legrand and Maylise Nastar for the critical reading of the manuscript.

APPENDIX: DIFFUSION COEFFICIENTS

In the Monte Carlo simulations *A* and *B* diffusion coefficients can be directly measured in solid solutions of various compositions (by measurements of $D_i = \langle R^2 \rangle_i / 6t^*$, where *R* is the displacement of some *i* tracer atoms). However, for very dilute alloys, analytic expressions can be obtained. In the case of one *B* atom in pure *A*, the corresponding impurity diffusion coefficient D_B^A depends on few particular exchange frequencies:[36,37] Γ_0 for an *A*-*V* exchange in pure *A* (i.e., far from the *B* atom), Γ_2 for the *B*-*V* exchange, Γ_3 for an *A*-*V* exchange near a *B* atom which dissociates a *B*-*V* pair, Γ_4 for an *A*-*V* exchange near a *B* atom which associates a *B*-*V* pair.

The *A* self-diffusion coefficient is $D_A^A = a^2 C_v f_0 \Gamma_0$ (where the correlation factor f_0 is a constant, $f_0 \simeq 0.72$ for the bcc lattice) and the expression of D_B^A is[36]

$$D_B^A = a^2 C_v \frac{\Gamma_4}{\Gamma_3} f_2 \Gamma_2, \tag{A1}$$

where *a* is the lattice parameter, C_v is the vacancy concentration, and $C_v \Gamma_4 / \Gamma_3$ can be interpreted as the local vacancy concentration near the solute *B* atom. f_2 is the correlation factor for *B*-*V* exchanges. It is due to the fact that if $\Gamma_2 \gg \Gamma_3$ (the vacancy jump frequency is much more higher with *B* than with *A* atoms), successive *B* jumps are highly correlated. In the frame of the so-called ''model II'' for the bcc structure,[36] f_2 is given by $f_2 = 7F\Gamma_3 / (2\Gamma_2 + 7F\Gamma_3)$, where $7F$ is a function of the Γ_4/Γ_0 ratio.

The Γ_0, Γ_2, Γ_3, and Γ_4 jump frequencies can be directly computed from the sets of parameters of Table I. A numerical expression of $7F$[38] gives $7F \simeq 4$, with the first and $7F \simeq 5$ with the second one. Moreover, in the first case $\Gamma_2 \gg \Gamma_3$ (then $f_2 \simeq 2\Gamma_3/\Gamma_2 \ll 1$) while with set 2: $\Gamma_2 = \Gamma_3$ ($f_2 \simeq 5/7$, the successive *B* jumps are almost uncorrelated). Finally, one gets $D_B^A = 2a^2 C_v \Gamma_4$ with set 1, $D_B^A = 5/7 a^2 C_v \Gamma_2$ with set 2, i.e., with the values of Table I, the same preexponential factor and the same migration energy for *B* atoms in pure *A*: 0.905 eV. The migration energy for *A* in pure

A are 1.075 eV with the first set of parameters, 0.99 eV with the second one.

In our Monte Carlo simulations we have to consider the diffusion of *B* atoms in an *A*-*B* alloy rather than in pure *A*. However as long as the *B* concentration is small, one can expect that Eq. (A1) is still valid, i.e., $D_B^{\alpha}=D_B^{A}$. This has been directly checked in the Monte Carlo simulations by measurements of $D_B=\langle R^2\rangle_B/6t^*$.

[1] G. Martin, in *Solid State Phase Transformations in Metals and Alloys* (Editions de Physique, Orsay, 1978), p. 337.

[2] J. W. Christian, *Transformations in Metals and Alloys* (Pergamon Press, Oxford, 1975), Chap. 10.

[3] F.F. Abraham, *Homogeneous Nucleation Theory* (Academic Press, New York, 1973).

[4] J. Feder, K.C. Russell, J. Lothe, and G.M. Pound, Adv. Phys. **15**, 111 (1966).

[5] K.C. Russell, Adv. Colloid Interface Sci. **13**, 205 (1980).

[6] J. Schmeltzer, in *Aggregation Phenomena in Complex Systems*, edited by J. Schmeltzer, G. Röpke, and R. Mahnke (Wiley, Weinheim, 1999), Chap. 2.

[7] R. Wagner and R. Kampmann, in *Phase Transformations in Materials*, edited by P. Haasen (VCH, Weinheim, 1991), Chap. 4.

[8] H. Löffler and H. G. Fabian, in *Structure and Structure Development of Al-Zn Alloys*, edited by H. Löffler (Akademic Verlag, Berlin, 1995), p. 345.

[9] K.F. Kelton, A.L. Greer, and V.C. Thompson, J. Chem. Phys. **79**, 6261 (1983).

[10] H. Wakeshima, J. Chem. Phys. **22**, 1614 (1954).

[11] K. Binder, Phys. Rev. B **15**, 4425 (1977); P. Mirold and K. Binder, Acta Metall. **25**, 1435 (1977).

[12] R. D. Doherty, ''Diffusive Phase Transformations in the Solid State,'' in *Physical Metallurgy*, edited by W. Cahn and P. Haasen (North-Holland, Amsterdam, 1996), Vol. 2, p. 1363.

[13] I.S. Servi and D. Turnbull, Acta Metall. **14**, 231 (1966).

[14] D.T. Wu, Solid State Phys. **50**, 13 (1997).

[15] D.W. Heerman, Phys. Rev. Lett. **50**, 1062 (1983).

[16] V.A. Shneidman, K.A. Jackson, and K.M. Beatty, Phys. Rev. B **59**, 3579 (1999).

[17] G. Martin, Phys. Rev. **41**, 2279 (1990).

[18] M. Nastar, P. Bellon, G. Martin, and J. Ruste, in *Phase Transformations and Systems Driven Far From Equilibrium*, edited by E. Ha, P. Bellon, M. Atzmon, and R. Trivedi, MRS Symposia Proceedings No. 481 (Materials Research Society, Pittsburgh, 1998).

[19] V.Y. Dobretsov, G. Martin, F. Soisson, and V.G. Vaks, Europhys. Lett. **31**, 417 (1995); V.Y. Dobretsov, V.G. Vaks, and G. Martin, Phys. Rev. B **54**, 3227 (1996).

[20] F. Soisson, A. Barbu, and G. Martin, Acta Mater. **44**, 3789 (1996).

[21] M. Athènes, Acta Mater (to be published); M. Athènes, Ph.D. thesis, Université de Paris VI, 1997; M. Athènes, F. Soisson, P. Bellon, and G. Martin, in *Solid-Solid Phase Transformations*, Proceedings of the International Conference, Kyoto, Japan, PTM 1999, edited by M. Koiwa, K. Otsuka, and T. Miyazaki (JIM, 1999), p. 433.

[22] D. Frenkel and B. Smit, in *Understanding Molecular Simulation* (Academic Press, San Diego, 1996), Chap. 5.

[23] C. Pareige, F. Soisson, G. Martin, and D. Blavette, Acta Mater. **47**, 1889 (1999).

[24] J.W. Cahn and J. Hilliard, J. Chem. Phys. **28**, 258 (1958).

[25] A. Finel, in *Statics and Dynamics of Alloy Phase Transformations*, edited by P.E.A. Turchi and A. Gonis (Plenum Press, New York, 1994), p. 495.

[26] A. Perini, G. Jacucci, and G. Martin, Phys. Rev. B **29**, 2689 (1984).

[27] M. Asta, S.M. Foiles, and A.A. Quong, Phys. Rev. B **57**, 11 265 (1998).

[28] M. Athènes and P. Bellon, Philos. Mag. **79**, 2243 (1999).

[29] V. Yu Dobretsov and V.G. Vaks, J. Phys.: Condens. Matter **10**, 2261 (1998); **10**, 2275 (1998).

[30] C. Frontera, E. Vives, T. Castan, and A. Planes, Phys. Rev. B **53**, 2886 (1996); P. Fratzl and O. Penrose, *ibid.* **53**, 1890 (1996); **55**, 6101 (1998); T.T. Rautiainen and A.P. Sutton, *ibid.* **59**, 13 681 (1999).

[31] M.E. Thompson, C.S. Su, and P.W. Voorhees, Acta Metall. Mater. **42**, 2107 (1994).

[32] *Phase Transformations and Evolution in Materials*, edited by P.E.A. Turchi and A. Gonis (TMS, Warrendale, 2000).

[33] A. Finel, in Ref. 32, p. 371.

[34] J.K. Lee, Mater. Sci. Eng., A **238**, 1 (1997).

[35] P. Fratzl and O. Penrose, Acta Metall. Mater. **43**, 2921 (1995).

[36] J. Philibert, *Atom Movements, Diffusion and Mass Transport in Solids* (Editions de physique, Les Ulis, 1991).

[37] A.R. Allnatt and A.B. Lidiard, *Atomic Transport in Solids* (Cambridge University Press, Cambridge, 1993).

[38] J.-L. Bocquet, G. Brebec, and Y. Limoge, in *Physical Metallurgy*, edited by R.W. Cahn and P. Haasen (North-Holland, Amsterdam, 1996), Chap. 7.